Al-Farouk journal of sciences
Volume (2), Issue (4) (Spt, 2026)
ISSN: 3135-2359

مجلة الفاروق للعلوم
المجلد (2) العدد 4 سبتمبر 2026
ردمد: 3135-2359

Mathematical Analysis of a Nonlinear Oscillator with Cubic Velocity Damping: Equilibrium, Stability, and Phase Curves

Fatima Al-Senussi Yasku
Department of Mathematics, Faculty of Economics and Accounting
Fezzan University, Libya
Email: fati.yasku@fezzanu.edu

Received: 15/8/2026 Revised: 17/8/2026 Accepted:* 05/9/*2026 Publication:* 29/10/*2026

Abstract

This paper examines the free response of a nonlinear oscillator that combines linear and cubic velocity damping with hardening cubic stiffness. The analysis identifies the equilibrium and its local behavior, then uses a mechanical-energy Lyapunov function and LaSalle's invariance principle to establish global asymptotic stability when the mass and linear stiffness are positive, the nonlinear stiffness and damping coefficients are nonnegative, and at least one damping mechanism is active. Numerical simulations with the DOP853 solver compare three initial displacement levels with a reference model that omits cubic damping. Energy decreased throughout all simulated trajectories, consistent with the analytical energy balance. At the final simulation time, adding cubic damping reduced the remaining energy by approximately 9%, 32%, and 58% for initial displacements of 0.5, 1.0, and 1.5, respectively. A parameter sweep also showed lower response peaks and a modest delay in successive peaks as cubic damping increased. These effects were strongest during the large-amplitude part of the motion; near equilibrium, both cases followed the same linearized dynamics. The results are numerical and specific to the selected dimensionless parameters. The paper presents an application of established stability methods rather than a new stability theorem.

***Index Terms*—Cubic damping, Duffing oscillator, LaSalle invariance principle, Lyapunov function, nonlinear damping, numerical simulation, phase portrait, stability analysis.**

I. INTRODUCTION

Damped oscillators are among the most widely used models in mechanics, electronics and structural dynamics. In the classical linear model the dissipative force is proportional to velocity, which gives exponentially decaying oscillations with a damping ratio that is independent of amplitude [1], [2]. Many physical dissipation mechanisms, however, depend on velocity in a nonlinear way, and the restoring force is often stiffer than linear at large displacement. A compact model that captures both effects is the oscillator with a cubic restoring force (a Duffing-type stiffness) and an additional cubic velocity-damping term [3], [4].

The problem addressed here is the free (unforced) response of this model. Three questions are of practical interest: where the system can come to rest, whether it returns to rest from any initial state, and how the cubic damping term changes the transient. The first two are mathematical questions that can be answered with phase-plane analysis, linearization and Lyapunov's direct method [2], [5], [6]. The third depends on amplitude and parameter values and is best studied with accurate numerical integration.

The objective of this study is to give a complete and verifiable treatment of these questions for one well-defined model and parameter set. The model, its stability analysis by an energy

function, and the use of LaSalle's principle are all standard; no claim of a new theoretical result is made. The contribution is the organized combination of the following elements:

1. a derivation, with every intermediate step, of the equilibria, the Jacobian matrix, the eigenvalues and the energy-rate identity for the model with both linear and cubic damping;
2. a proof of global asymptotic stability via LaSalle's invariance principle, with explicit statement of the parameter conditions under which each step holds and of what fails when they do not;
3. a reproducible numerical study with stated solver settings, comparing $\gamma = 0.08$ with $\gamma = 0$ for three initial conditions and including a sweep over γ;
4. numerical checks that link the simulations back to the analysis: monotone energy decay, agreement of the computed energy rate with $-cv^2 - \gamma v^4$, an integrated energy balance, and a tolerance-refinement test.

Section II reviews related work. Section III states the model and assumptions. Sections IV and V contain the local and global stability analysis. Section VI describes the numerical method, Section VII presents the results, Section VIII discusses limitations, and Section IX concludes.

II. Related Work

A. Stability Theory for Nonlinear Systems

The direct method of Lyapunov, introduced in his 1892 thesis and available in English translation [5], establishes stability by finding a scalar function that decreases along trajectories without solving the equations. For mechanical systems the total energy is a natural candidate. A difficulty arises when the energy derivative is only negative semidefinite, as happens for velocity-dependent damping, because the derivative vanishes whenever the velocity is zero. LaSalle's invariance principle [6] resolves this by showing that bounded trajectories approach the largest invariant set in which the derivative vanishes. Modern textbook treatments, including the Barbashin–Krasovskii form of this result and linearization through the Hartman–Grobman theorem, are given in [2] and [1]. Classical perturbation methods for weakly nonlinear oscillators, including averaging and multiple scales applied to damped Duffing equations, are covered in [3], and a broad survey of Duffing-type behavior is collected in [4].

B. Nonlinear Damping: Physical Origins and Engineering Use

Nonlinear damping appears in systems at very different scales. In nanomechanical resonators made from carbon nanotubes and graphene, Eichler *et al.* [7] showed that a nonlinear damping term was needed to describe the measured response, and Catalini *et al.* [8] modelled and observed nonlinear damping in dissipation-diluted silicon-nitride membranes, linking it to geometric nonlinearity. In vibration isolation, Lang *et al.* [9] studied theoretically how nonlinear viscous damping changes the transmissibility of single-degree-of-freedom systems, and Xiao, Jing and Cheng [10] examined isolators with cubic nonlinear damping under force and base excitation. For free vibration, Tang and Brennan [11] compared several nonlinear damping mechanisms and reported that cubic damping attenuates free vibration less effectively than quadratic damping. Elliott, Ghandchi Tehrani and Langley [12] reviewed nonlinear damping and quasi-linear (equivalent-linear) modelling, which underlies the amplitude-dependent damping estimate used in Section V-F. More recently, Zhu and Lang [13]

analyzed antisymmetric nonlinear damping for energy harvesting and isolation under general inputs.

C. Analysis of Damped Duffing-Type Oscillators

A large recent literature develops approximate analytical solutions for damped Duffing-type equations and checks them against numerical integration. El-Dib [14] treated a damped Helmholtz–Rayleigh–Duffing oscillator with a non-perturbative approach and derived stability conditions from the resulting frequency relation. Salas [15] gave exact and elementary approximate solutions of the linearly damped Duffing equation and compared them with Runge–Kutta solutions. Moatimid, Amer and Amer [16] analyzed a forced, linearly damped Duffing oscillator with time-delayed feedback. Alluhydan *et al.* [17] studied an excited Duffing oscillator whose equation of motion contains both linear and pure cubic damping terms together with delayed feedback, and Abohamer *et al.* [18] examined chaotic and stability behavior of a viscously damped Duffing oscillator under sinusoidal forcing. At the device level, Kakou, Gupta and Barry [19] analyzed the stability of a Duffing oscillator coupled to a nonlinear electromagnetic absorber–inerter using harmonic balance, Floquet theory and Lyapunov exponents.

D. Position of the Present Study

Most of the works above concern forced response, frequency-domain transmissibility, or approximate analytical solutions. The unforced model with simultaneous linear and cubic velocity damping and hardening stiffness is simpler, and its global stability follows from standard theory [2], [6]. The present paper does not extend that theory. It provides a self-contained derivation for this specific model, makes the role of each parameter condition explicit, and couples the analysis to numerical evidence that can be reproduced from the accompanying program.

III. MATHEMATICAL MODEL AND ASSUMPTIONS

A. Governing Equation

The oscillator studied is

$$m\ddot{x} + c\dot{x} + \gamma\dot{x}^3 + kx + \alpha x^3 = 0 \tag{1}$$

where $x(t)$ is the displacement, $\dot{x}$ the velocity, $\ddot{x}$ the acceleration, m the mass, c the linear damping coefficient, γ the cubic damping coefficient, k the linear stiffness and α the coefficient of the cubic stiffness nonlinearity. All signs are as given; with positive coefficients each damping term opposes the motion and each stiffness term acts toward the origin. The case $\alpha > 0$ corresponds to a hardening spring.

The nominal values used throughout the numerical study are

$$m = 1, \quad c = 0.15, \quad \gamma = 0.08, \quad k = 1, \quad \alpha = 0.40 \tag{2}$$

These are representative simulation values chosen to give a lightly damped, mildly nonlinear response. They are not measured properties of a physical device.

B. Dimensional Consistency and Normalization

If (1) is read in SI units, every term must have the unit of force (N). With x in m and t in s, this requires $[m]$ = kg, $[c] = \mathrm{N\,s\,m^{-1}}$, $[\gamma] = \mathrm{N\,s^3\,m^{-3}}$, $[k] = \mathrm{N\,m^{-1}}$ and $[\alpha] = \mathrm{N\,m^{-3}}$, so that $c\dot{x}$, $\gamma\dot{x}^3$, kx and αx^3 are all in newtons. In this paper the variables are instead taken as nondimensional. Introducing a length scale L, the natural frequency $\omega_n = \sqrt{k/m}$, and $x = L\tilde{x}$, $\tau = \omega_n t$, then dividing (1) by kL gives

$$\tilde{x}'' + 2\zeta\tilde{x}' + \tilde{\gamma}\,\tilde{x}'^3 + \tilde{x} + \tilde{\alpha}\,\tilde{x}^3 = 0, \qquad 2\zeta = \frac{c}{\sqrt{mk}}, \quad \tilde{\gamma} = \frac{\gamma L^2 \omega_n^3}{k}, \quad \tilde{\alpha} = \frac{\alpha L^2}{k} \tag{3}$$

where primes denote derivatives with respect to τ. All groups in (3) are dimensionless. With $m = k = L = 1$ one has $\omega_n = 1$, $\tau = t$, $2\zeta = c$, $\tilde{\gamma} = \gamma$ and $\tilde{\alpha} = \alpha$, so the values in (2) can be read directly as the dimensionless coefficients. Time is therefore measured in units of $1/\omega_n$; the label "s" used in the program and figures refers to this nondimensional time unit.

C. First-Order State-Space Form

Defining the velocity $v = \dot{x}$ and dividing by $m > 0$ converts (1) into the autonomous first-order system

$$\begin{aligned} \dot{x} &= v \\ \dot{v} &= -\frac{1}{m}(cv + \gamma v^3 + kx + \alpha x^3) \end{aligned} \tag{4}$$

with state $\mathbf{z} = (x, v)^{\mathsf{T}} \in \mathbb{R}^2$. The right-hand side $\mathbf{f}(\mathbf{z})$ of (4) is a polynomial and hence continuously differentiable, so solutions exist and are unique for every initial state; Section V shows they also remain bounded for all $t \geq 0$ under the stated conditions.

D. Assumptions

The analysis uses the following assumptions, which hold for the nominal values (2): (A1) $m > 0$ and $k > 0$; (A2) $\alpha \geq 0$; (A3) $c \geq 0$ and $\gamma \geq 0$; (A4) $c + \gamma > 0$, i.e., at least one damping mechanism is active. The system is autonomous (no external forcing), parameters are constant, and the model is deterministic. The consequences of relaxing (A2)–(A4) are discussed in Section V-E.

IV. Equilibrium and Local Stability Analysis

A. Equilibrium Points

Equilibria satisfy $\mathbf{f}(\mathbf{z}^*) = \mathbf{0}$. The first equation of (4) gives $v^* = 0$. Substituting into the second gives

$$kx^* + \alpha x^{*3} = x^*(k + \alpha x^{*2}) = 0 \tag{5}$$

Under (A1)–(A2), $k + \alpha x^{*2} \geq k > 0$, so the only solution is $x^* = 0$. The system therefore has the unique equilibrium $(x^*, v^*) = (0,0)$. The damping coefficients do not enter (5) because damping forces vanish at zero velocity. If instead $\alpha < 0$ (softening spring), two additional equilibria $x^* = \pm\sqrt{-k/\alpha}$ appear; this case is outside the assumptions of the paper.

B. Jacobian Matrix

The Jacobian of (4) at an arbitrary state is

$$\mathbf{J}(x, v) = \begin{bmatrix} \frac{\partial \dot{x}}{\partial x} & \frac{\partial \dot{x}}{\partial v} \\ \frac{\partial \dot{v}}{\partial x} & \frac{\partial \dot{v}}{\partial v} \end{bmatrix} = \begin{bmatrix} 0 & 1 \\ -\frac{k + 3\alpha x^2}{m} & -\frac{c + 3\gamma v^2}{m} \end{bmatrix} \tag{6}$$

Evaluating at the equilibrium $(0,0)$ gives

$$\mathbf{J}_0 = \mathbf{J}(0,0) = \begin{bmatrix} 0 & 1 \\ -\frac{k}{m} & -\frac{c}{m} \end{bmatrix}, \qquad \mathrm{tr}\mathbf{J}_0 = -\frac{c}{m}, \qquad \det\mathbf{J}_0 = \frac{k}{m} \tag{7}$$

Both nonlinear coefficients disappear from $\mathbf{J}_0$: the term $3\alpha x^2$ vanishes at $x = 0$ and the term $3\gamma v^2$ vanishes at $v = 0$. The linearization at the origin is therefore identical to that of the linear damped oscillator $m\ddot{x} + c\dot{x} + kx = 0$.

C. Eigenvalues and Local Stability

The characteristic equation $\det(\lambda\mathbf{I} - \mathbf{J}_0) = 0$ is

$$\lambda^2 + \frac{c}{m}\lambda + \frac{k}{m} = 0 \quad \Rightarrow \quad \lambda_{1,2} = \frac{-c \pm \sqrt{c^2 - 4mk}}{2m} \tag{8}$$

For $c > 0$, $\mathrm{tr}\mathbf{J}_0 < 0$ and $\det\mathbf{J}_0 > 0$, so both eigenvalues have negative real parts. Writing $\omega_n = \sqrt{k/m}$ and $\zeta = c/\left(2\sqrt{mk}\right)$, the eigenvalues are complex when $\zeta < 1$:

$$\lambda_{1,2} = -\zeta\omega_n \pm i\,\omega_n\sqrt{1-\zeta^2} \tag{9}$$

For the nominal values (2), $c^2 - 4mk = 0.0225 - 4 = -3.9775 < 0$, $\zeta = 0.075$, and

$$\lambda_{1,2} = -0.075 \pm 0.99718\,i \tag{10}$$

These values, listed in Table I, were also confirmed numerically by the program. Since the real parts are nonzero, the equilibrium is hyperbolic and the Hartman–Grobman theorem [1], [2] implies that the nonlinear system is locally topologically equivalent to its linearization near the origin. The origin is a stable focus: nearby trajectories spiral into it, and it is locally exponentially stable with rate $\zeta\omega_n = 0.075$ for the amplitude.

TABLE I

LINEARIZATION AT THE EQUILIBRIUM FOR THE NOMINAL PARAMETERS

Quantity	Expression	Value
Trace of $\mathbf{J}_0$	$-c/m$	-0.15
Determinant of $\mathbf{J}_0$	k/m	1.00
Discriminant	$c^2 - 4mk$	-3.9775
Natural frequency	$\omega_n = \sqrt{k/m}$	1.0000
Damping ratio	$\zeta = c/\left(2\sqrt{mk}\right)$	0.0750
Eigenvalues	$-\zeta\omega_n \pm i\omega_n\sqrt{1-\zeta^2}$	$-0.0750 \pm 0.99718\,i$
Linear amplitude factor at $t = 30$	$e^{-\zeta\omega_n \cdot 30}$	0.1054
Linear energy factor at $t = 30$	$e^{-2\zeta\omega_n \cdot 30}$	0.0111

D. Role of Cubic Damping in the Linearization

Because γ does not appear in (7)–(8), linear analysis predicts the same local decay rate for $\gamma = 0.08$ and $\gamma = 0$. The cubic damping force γv^3 is of third order in the state and is negligible compared with cv when $|v| \ll \sqrt{c/\gamma}$; for the nominal values $\sqrt{c/\gamma} = \sqrt{1.875} \approx 1.37$. Its effect must therefore be sought in the large-amplitude part of the transient, which is examined numerically in Section VII.

The linearization is also inconclusive in one boundary case. If $c = 0$ and $\gamma > 0$, then $\lambda_{1,2} = \pm i\sqrt{k/m}$, the equilibrium is non-hyperbolic, and the linear model predicts undamped oscillation. Stability in that case cannot be decided from eigenvalues; it follows from the energy analysis of Section V, which covers $c = 0$ through assumption (A4).

V. LYAPUNOV AND ENERGY ANALYSIS

A. Energy Function

The candidate Lyapunov function is the total mechanical energy, the sum of kinetic energy and the potential energy of the restoring force $kx + \alpha x^3$:

$$E(x,v) = \tfrac{1}{2}mv^2 + \tfrac{1}{2}kx^2 + \tfrac{1}{4}\alpha x^4 \tag{11}$$

The potential term satisfies $\frac{\mathrm{d}}{\mathrm{d}x}\left(\frac{1}{2}kx^2 + \frac{1}{4}\alpha x^4\right) = kx + \alpha x^3$, which confirms that (11) is the correct energy for the stiffness in (1). For the nominal parameters, $E = \frac{1}{2}v^2 + \frac{1}{2}x^2 + 0.1x^4$.

B. Derivative Along Trajectories

Differentiating (11) along solutions of (4) with the chain rule gives

$$\dot{E} = \frac{\partial E}{\partial x}\dot{x} + \frac{\partial E}{\partial v}\dot{v} = (kx + \alpha x^3)v + mv \cdot \left[-\tfrac{1}{m}(cv + \gamma v^3 + kx + \alpha x^3)\right] \tag{12}$$

The conservative terms $(kx + \alpha x^3)v$ cancel exactly, leaving

$$\dot{E} = -cv^2 - \gamma v^4 = -v^2(c + \gamma v^2) \tag{13}$$

This verifies the energy-rate relation for the model. The expression shows that the instantaneous dissipated power equals the product of velocity and the total damping force $cv + \gamma v^3$, and that the cubic term behaves like an amplitude-dependent viscous coefficient $c + \gamma v^2$. Integrating (13) from 0 to t gives the energy balance

$$E(t) = E(0) - \int_0^t \big(c\, v^2(s) + \gamma\, v^4(s)\big)\, \mathrm{d}s \tag{14}$$

which is used as a numerical check in Section VII.

C. Sign Conditions and Properties of E

Non-positivity of $\dot{E}$. Since $v^2 \geq 0$ and $v^4 \geq 0$, (13) gives $\dot{E} \leq 0$ for all states whenever $c \geq 0$ and $\gamma \geq 0$ (assumption A3). If, in addition, $c + \gamma > 0$ (A4), then $c + \gamma v^2 > 0$ for every $v \neq 0$, so

$$\dot{E} = 0 \Leftrightarrow v = 0 \tag{15}$$

$\dot{E}$ is therefore negative semidefinite, not negative definite: it vanishes on the entire x-axis, including points with $x \neq 0$. The standard Lyapunov theorem then yields only stability, not asymptotic stability, which is why LaSalle's principle is needed.

Positive definiteness and radial unboundedness of E. Under (A1)–(A2), each term in (11) is non-negative and $E(x, v) \geq \frac{1}{2}mv^2 + \frac{1}{2}kx^2 > 0$ for $(x, v) \neq (0,0)$, while $E(0,0) = 0$. The same lower bound shows $E \to \infty$ as $\| (x, v) \| \to \infty$, so E is radially unbounded and every sublevel set $\Omega_\rho = \{(x, v): E(x, v) \leq \rho\}$ is closed and bounded, hence compact.

D. Global Asymptotic Stability by LaSalle's Principle

Proposition. Under assumptions (A1)–(A4), the equilibrium $(0,0)$ of (4) is globally asymptotically stable.

Proof. The argument follows LaSalle's invariance principle [6] in the form given in [2].

1. *Stability.* E is positive definite and $\dot{E} \leq 0$, so E is a Lyapunov function and the origin is stable in the sense of Lyapunov [2], [5].
2. *Compact positively invariant set.* Take any initial state $\mathbf{z}_0$ and let $\rho = E(\mathbf{z}_0)$. Since $\dot{E} \leq 0$, $E\big(\mathbf{z}(t)\big) \leq \rho$ for all $t \geq 0$, so the trajectory stays in the compact set Ω_ρ. Hence the solution is bounded and defined for all $t \geq 0$, and Ω_ρ is positively invariant.
3. *Set where* $\dot{E} = 0$. By (15), $S = \{\mathbf{z} \in \Omega_\rho : \dot{E}(\mathbf{z}) = 0\} = \{(x, 0) \in \Omega_\rho\}$.
4. *Largest invariant subset of* S. Let $\mathbf{z}(t)$ be a solution that remains in S for all t. Then $v(t) \equiv 0$, hence $\dot{v}(t) \equiv 0$, and the second equation of (4) gives $kx(t) + \alpha x(t)^3 \equiv 0$. By (5) and (A1)–(A2), $x(t) \equiv 0$. The largest invariant set in S is therefore $M = \{(0,0)\}$.
5. *Conclusion.* By LaSalle's principle, every solution starting in Ω_ρ converges to M as $t \to \infty$. Because ρ was arbitrary and E is radially unbounded, this holds for every initial state. Combined with step 1, the origin is globally asymptotically stable. ■

The proof uses only the signs of the coefficients. It does not require $c > 0$; for $c = 0$ and $\gamma > 0$, the case in which linearization fails (Section IV-D), the origin is still globally asymptotically stable. In that case the decay is not exponential: first-order averaging [3] predicts an amplitude that decreases algebraically, roughly as $t^{-1/2}$, rather than as $e^{-\zeta\omega_n t}$. When $c > 0$, local exponential stability (Section IV-C) and global asymptotic stability hold together.

E. Summary of Conditions and Their Role

Table II summarizes where each condition is used and what changes when it is violated. If $\gamma < 0$ with $c > 0$, (13) gives $\dot{E} > 0$ for $|v| > \sqrt{c/|\gamma|}$, so energy can grow at high speed; the origin remains locally asymptotically stable (the linearization is unchanged), but the global argument fails. If $\alpha < 0$, E is not radially unbounded and additional equilibria exist, so only local results can be obtained.

TABLE II

PARAMETER CONDITIONS USED IN THE STABILITY ANALYSIS

Condition	Where it is used	Consequence if violated
$m > 0, k > 0$	Unique equilibrium; E positive definite; $\det \mathbf{J}_0 > 0$	$k < 0$: origin becomes a saddle
$\alpha \geq 0$	Unique equilibrium; E radially unbounded	$\alpha < 0$: extra equilibria $\pm\sqrt{-k/\alpha}$; only local stability
$c \geq 0, \gamma \geq 0$	$\dot{E} \leq 0$ everywhere	$\gamma < 0$: $\dot{E} > 0$ for $\lvert v \rvert > \sqrt{c/\lvert\gamma\rvert}$
$c + \gamma > 0$	$\dot{E} = 0$ only on $v = 0$ (LaSalle step 3)	$c = \gamma = 0$: energy conserved, closed orbits (center)
$c > 0$	Hyperbolic eigenvalues; local exponential decay	$c = 0, \gamma > 0$: GAS holds but decay is not exponential

F. Amplitude-Dependent Equivalent Damping

A simple quasi-linear estimate [3], [12] explains why cubic damping matters more at larger amplitude. Assume a nearly harmonic motion $x \approx A\cos\omega t$, $v \approx -A\omega\sin\omega t$. Equating the energy dissipated per cycle by $cv + \gamma v^3$ with that of an equivalent viscous damper $c_{\mathrm{eq}} v$, and using $\int_0^{2\pi} \sin^4\theta \, \mathrm{d}\theta = 3\pi/4$, gives

$$c_{\mathrm{eq}}(A) = c + \frac{3}{4}\gamma A^2 \omega^2 \tag{16}$$

With $\omega \approx 1$ and the nominal values, $c_{\mathrm{eq}}/c \approx 1 + 0.4A^2$, i.e., about 1.1, 1.4 and 1.9 for $A = 0.5$, 1.0 and 1.5. This is an approximation, valid only for weak damping and nearly harmonic motion, and is used here only to interpret the numerical results, not as a proof.

VI. NUMERICAL METHOD AND SIMULATION SETUP

A. Solver and Settings

System (4) was integrated with the explicit Runge–Kutta method of order 8 by Dormand and Prince (DOP853) [20], [21], as implemented in `scipy.integrate.solve_ivp` [22]. The settings, identical to those of the attached program, were: relative tolerance $\mathrm{rtol} = 10^{-9}$, absolute tolerance $\mathrm{atol} = 10^{-11}$, adaptive internal step size, time interval $[0,30]$, and dense output evaluated on a uniform grid with spacing $\Delta t = 0.01$ (3001 samples). Computations used Python 3.13 with NumPy 2.5.3 [23], SciPy 1.18.1 [22] and Matplotlib 3.11.2 [24].

B. Cases Studied

The nominal parameters (2) were used with initial conditions $(x_0, v_0) = (1.0,0)$, $(1.5,0)$ and $(0.5,0)$. Each case was solved with $\gamma = 0.08$ and with $\gamma = 0$, all other parameters and initial conditions unchanged; note that the $\gamma = 0$ case retains the linear damping $c = 0.15$ and the cubic stiffness $\alpha = 0.40$. In addition, for $(x_0, v_0) = (1.5,0)$ the cubic damping coefficient was varied over $\gamma \in \{0,0.04,0.08,0.16,0.32,0.64\}$.

C. Output Quantities and Checks

For each run the program records $x(t)$, $v(t)$ and $E(t)$ from (11), the final state and energy at $t = T = 30$, the ratio $E(T)/E(0)$, the first positive displacement peak after release, and a settling time defined as the first instant after which $\sqrt{x^2 + v^2} < 0.02$ for the rest of the interval. Four checks connect the computation with the analysis: (i) E is non-increasing on the output grid (successive differences $\leq 10^{-12}$); (ii) a second-order central difference of the sampled $E(t)$ is compared with the analytical rate (13); (iii) the integrated balance (14) is evaluated with the trapezoidal rule; and (iv) each $\gamma = 0.08$ run is repeated with $\mathrm{rtol} = 10^{-12}$, $\mathrm{atol} = 10^{-14}$ to bound the integration error.

D. Relation to the Attached Files

The attached program and result files were used as the primary source. Re-running the attached program reproduced its time-series file exactly at the printed precision (all 3001 rows), and its summary values agree with the extended program to all printed digits. The extended program keeps the same

model, parameters, solver and tolerances and adds the $\gamma = 0$ summary for all initial conditions, the γ sweep, the checks (ii)–(iv), and figures exported at 300 dpi (PNG) and as vector PDF/SVG without in-plot titles. Because the 2% settling threshold is not reached within 30 time units in any run, settling times were additionally computed on an extended interval $[0,200]$ with the same settings; these values are reported separately and labelled as supplementary.

VII. Results and Discussion

A. Time Response

Fig. 1 shows the displacement for $(x_0, v_0) = (1,0)$ with and without cubic damping. Both responses are decaying oscillations about $x = 0$ with a period close to $2\pi/\omega_d \approx 6.3$, consistent with (10). The cubic term reduces every extremum: the first trough is -0.764 instead of -0.823 and the first positive peak after release is 0.593 instead of 0.670 (Table III). The difference between the curves is largest in the first cycles, where velocities are highest, and becomes smaller later, when both responses approach the small-amplitude regime governed by the common linearization (Section IV-D).

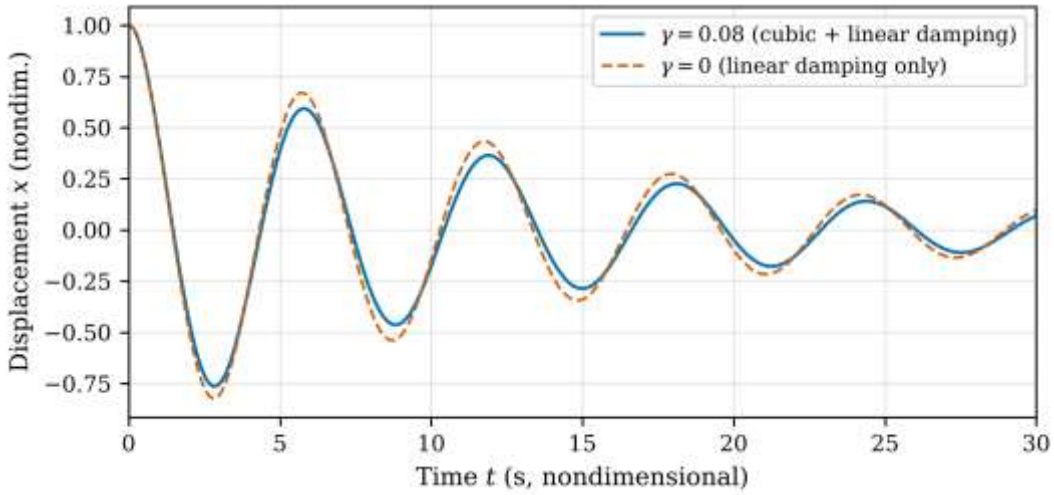

Fig. 1. Displacement $x(t)$ for $(x_0, v_0) = (1,0)$ with cubic damping ($\gamma = 0.08$, solid) and without it ($\gamma = 0$, dashed); $m = 1$, $c = 0.15$, $k = 1$, $\alpha = 0.40$ in both cases.

Table III lists the main quantities for all six runs. In every case the cubic term lowers the peak amplitudes, the maximum speed and the energy remaining at $t = 30$. The relative effect grows with initial amplitude: the ratio $E(T)|_{\gamma=0.08}/E(T)|_{\gamma=0}$ is 0.909 for $x_0 = 0.5$, 0.677 for $x_0 = 1.0$ and 0.418 for $x_0 = 1.5$, i.e., reductions of about 9%, 32% and 58%. This ordering agrees with the equivalent-damping estimate (16), which predicts the largest increase in effective damping for the largest amplitude. The agreement is qualitative; (16) is not used to predict the tabulated numbers.

TABLE III

Numerical Results for the Three Initial Conditions ($T = 30$)

x_0	γ	First trough	First peak	max|v|	$x(T)$	$v(T)$	$E(0)$	$E(T)$	$E(T)/E(0)$
1.0	0.08	−0.7642	0.5931	0.9519	0.06778	0.05748	0.60000	0.003952	0.00659
1.0	0	−0.8231	0.6698	0.9874	0.09499	0.05136	0.60000	0.005839	0.00973
1.5	0.08	−1.0853	0.8234	1.5132	0.11864	0.00033	1.63125	0.007057	0.00433
1.5	0	−1.2755	1.0691	1.6426	0.13312	−0.12632	1.63125	0.016870	0.01034
0.5	0.08	−0.3922	0.3085	0.4548	0.01185	0.04866	0.13125	0.001254	0.00955
0.5	0	−0.3997	0.3181	0.4589	0.01334	0.05081	0.13125	0.001380	0.01051

For $\gamma = 0$ the energy ratios $E(T)/E(0)$ lie between 0.0097 and 0.0105, close to the purely linear prediction $e^{-2\zeta\omega_n T} = 0.0111$ of Table I. Exact agreement is not expected, because $E(T)$ is sampled at a particular phase of the oscillation and the cubic stiffness alters the motion at larger amplitude.

B. Phase Curves

Fig. 2 shows the phase trajectories for $\gamma = 0.08$. All three curves spiral clockwise into the origin, as predicted for a stable focus (Section IV-C), and none crosses itself, as required for an autonomous planar system with unique solutions. The curves for different initial conditions do not intersect each other either. The trajectory from $(1.5,0)$ is visibly non-elliptical in its first loop, reflecting the hardening stiffness and the cubic damping at large amplitude; later loops become nearly elliptical as the motion approaches the linear regime. The successive crossings of the x-axis ($v = 0$) are the points where $\dot{E} = 0$ in (15); the trajectories pass through these points without stopping, as required by step 4 of the LaSalle argument.

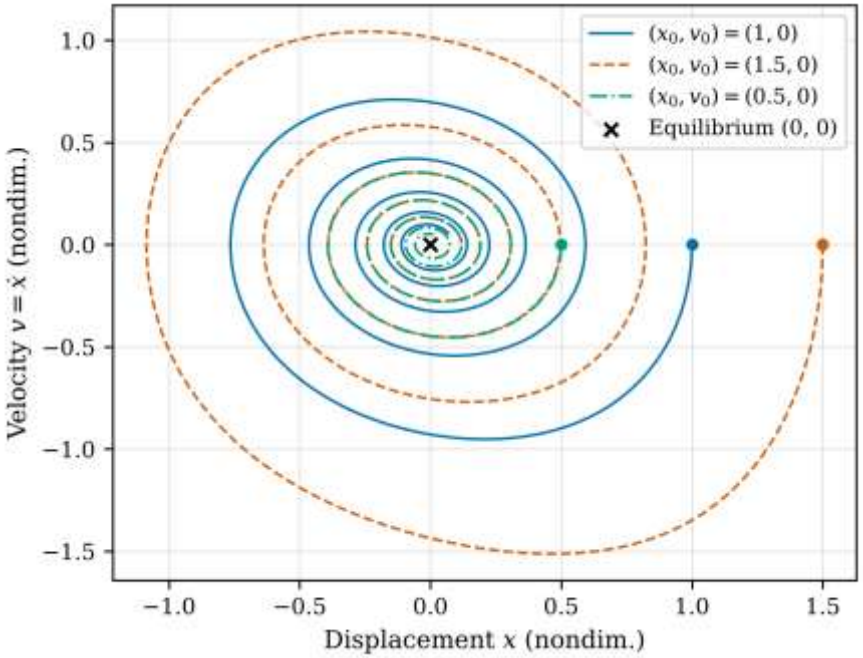

Fig. 2. Phase trajectories (x, v) for $\gamma = 0.08$ from the initial states $(1,0)$, $(1.5,0)$ and $(0.5,0)$ (dots) over $0 \le t \le 30$. The cross marks the equilibrium $(0,0)$.

C. Energy Decay and Verification of the Energy Rate

Fig. 3 shows $E(t)$ for $(x_0, v_0) = (1,0)$ on linear and logarithmic scales. Both curves decrease monotonically, in agreement with $\dot{E} \le 0$. They have a staircase shape: the energy drops quickly when $|v|$ is large and is almost flat near the turning points where $v = 0$, exactly as (13) implies. On the logarithmic scale, the $\gamma = 0.08$ curve separates from the $\gamma = 0$ curve mainly during the first two cycles; afterwards the two curves are nearly parallel, which indicates a similar exponential rate once the amplitude is small. This is the numerical counterpart of the observation in Section IV-D that γ does not affect the linearization.

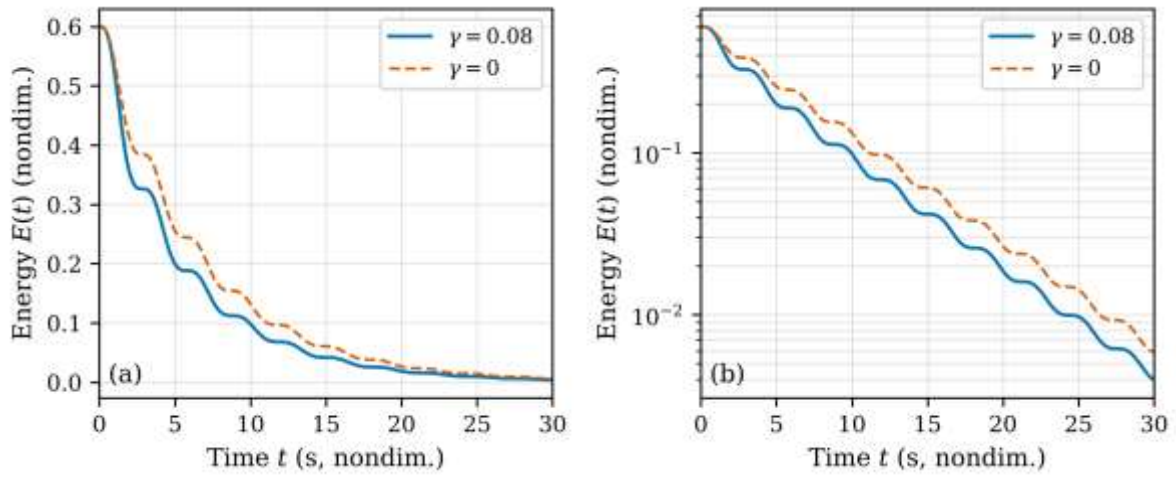

Fig. 3. Mechanical energy $E(t)$ for $(x_0, v_0) = (1,0)$ with $\gamma = 0.08$ (solid) and $\gamma = 0$ (dashed): (a) linear scale; (b) logarithmic scale.

Fig. 4 compares a finite-difference estimate of $\mathrm{d}E/\mathrm{d}t$ with the analytical expression $-cv^2 - \gamma v^4$ evaluated on the computed velocity; the curves coincide at plotting resolution. Table IV quantifies the checks for all six runs. The largest pointwise difference between the finite-difference and analytical rates is at most 6.0×10^{-5}, compared with a peak rate magnitude of about 0.2 in Fig. 4; this difference is consistent with the $O(\Delta t^2)$ truncation error of the difference formula. The integrated energy balance (14) holds to within 3.6×10^{-8}, and refining the tolerances by three orders of magnitude changes x and v by less than 2×10^{-9}. The numerical results are therefore not limited by integration error at the precision reported in the tables.

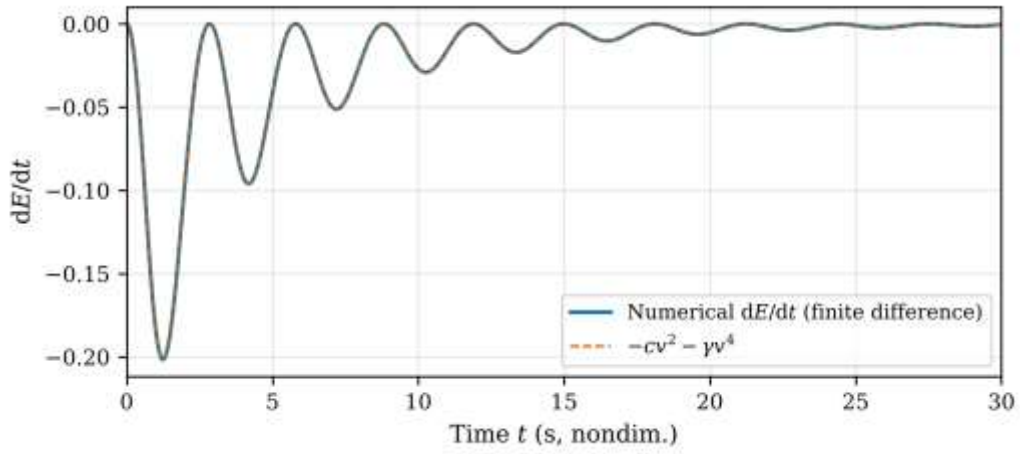

Fig. 4. Energy rate for $(x_0, v_0) = (1,0)$, $\gamma = 0.08$: central finite difference of the computed $E(t)$ (solid) and the analytical expression $-cv^2 - \gamma v^4$ from (13) (dashed).

TABLE IV

NUMERICAL CHECKS OF THE ENERGY ANALYSIS AND INTEGRATION ACCURACY

x_0	γ	E non-increasing	Max rate difference	Energy-balance error	Max $\lvert\Delta x\rvert$ (tol. refined)	Max $\lvert\Delta v\rvert$ (tol. refined)
1.0	0.08	Yes	9.9×10^{-6}	1.1×10^{-8}	6.9×10^{-10}	1.2×10^{-9}
1.5	0.08	Yes	6.0×10^{-5}	3.8×10^{-10}	9.7×10^{-10}	1.7×10^{-9}
0.5	0.08	Yes	1.5×10^{-6}	2.3×10^{-9}	4.8×10^{-10}	6.3×10^{-10}
1.0	0	Yes	9.8×10^{-6}	1.3×10^{-8}	—	—
1.5	0	Yes	4.0×10^{-5}	3.6×10^{-8}	—	—
0.5	0	Yes	1.5×10^{-6}	2.6×10^{-9}	—	—

D. Effect of the Cubic Damping Coefficient

Fig. 5 and Table V show the response from $(1.5,0)$ for six values of γ. Within this set, increasing γ reduces the first positive peak monotonically from 1.069 ($\gamma = 0$) to 0.403 ($\gamma = 0.64$), reduces the maximum speed from 1.643 to 1.168, and lowers the final energy ratio $E(T)/E(0)$ from 1.03×10^{-2} to 8.8×10^{-4}. Fig. 5(b) shows that most of the additional dissipation occurs in the first few cycles, after which the curves for different γ decay at similar logarithmic rates.

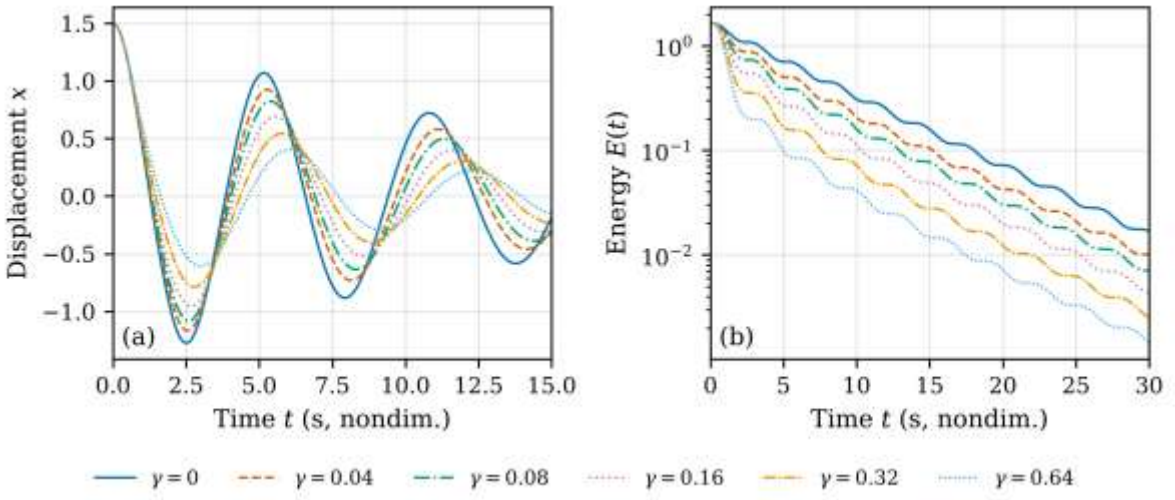

Fig. 5. Effect of the cubic damping coefficient for $(x_0, v_0) = (1.5,0)$: (a) displacement for $0 \le t \le 15$; (b) energy on a logarithmic scale for $0 \le t \le 30$. Other parameters as in (2).

TABLE V

EFFECT OF γ ON THE RESPONSE FROM $(x_0, v_0) = (1.5,0)$

γ	$E(10)$	$E(30)$	$E(30)/E(0)$	First peak time	First peak x	Second peak time	Second peak x	max$\lvert v\rvert$
0	0.3063	0.01687	0.01034	5.16	1.0691	10.81	0.7221	1.6426
0.04	0.2064	0.01010	0.00619	5.29	0.9237	11.12	0.5805	1.5702
0.08	0.1593	0.00706	0.00433	5.39	0.8234	11.33	0.4973	1.5132
0.16	0.1121	0.00437	0.00268	5.55	0.6907	11.60	0.3999	1.4263
0.32	0.0717	0.00253	0.00155	5.77	0.5428	11.93	0.3037	1.3089
0.64	0.0414	0.00144	0.00088	6.06	0.4033	12.29	0.2211	1.1682

The sweep also shows a systematic delay of the peaks: the first positive peak moves from $t = 5.16$ for $\gamma = 0$ to $t = 6.06$ for $\gamma = 0.64$. A plausible explanation, consistent with the hardening stiffness, is that the instantaneous oscillation frequency of a Duffing oscillator with $\alpha > 0$ increases with amplitude [3], [4]; stronger damping reduces the amplitude faster and therefore lowers the instantaneous frequency. The increased effective damping (16) also lengthens the damped period slightly. These explanations are offered as interpretations of the numerical observation and have not been separated quantitatively in this study.

E. Settling Behavior

With the 2% threshold on $\sqrt{x^2 + v^2}$, none of the six runs settles within $0 \le t \le 30$, in agreement with the original summary file. This is consistent with the linear estimate: the amplitude envelope decreases by only $e^{-0.075 \cdot 30} \approx 0.105$ over the interval (Table I). On the supplementary interval $[0,200]$, the settling times were 42.42, 50.75 and 53.71 for $\gamma = 0.08$ and 42.76, 53.41 and 59.11 for $\gamma = 0$, for $x_0 = 0.5$, 1.0 and 1.5, respectively. The reduction due to cubic damping is again largest for the largest initial displacement (5.4 time units) and smallest for the smallest (0.34). For comparison, a purely linear envelope decaying from 1 to 0.02 at rate 0.075 would require $\ln 50/0.075 \approx 52$ time units. Because this metric depends on the threshold and on the phase at which the norm crosses it, these values should be read only as indicative.

F. Mathematical Results Versus Numerical Observations

It is useful to separate what has been proved from what has been observed. The following statements are proved in Sections IV–V for all parameters satisfying (A1)–(A4) and all initial states: the origin is the unique equilibrium; the energy satisfies (13) and never increases; and the origin is globally asymptotically stable. For $c > 0$ it is also locally exponentially stable with eigenvalues independent of γ. The following are numerical observations valid only for the nominal parameters, the initial conditions and the time interval studied: the percentage reductions in remaining energy; the monotone dependence on γ within the sampled set; the delay of the peaks; and the settling times. The numerical checks in Table IV show that these observations are not artifacts of integration error, but they do not extend them to other parameter regions.

VIII. LIMITATIONS

The study has several limitations. First, the parameter values are nominal and nondimensional; no experimental data were used, and no identification of c, γ or α for a physical system was attempted. Second, only free vibration from rest ($v_0 = 0$) at three displacement levels was simulated; initial velocities, forced excitation, noise and parameter uncertainty were not considered, and the forced response, where cubic damping is known to affect transmissibility [9], [10], may behave differently. Third, the global result requires $\alpha \geq 0$ and non-negative damping; softening springs and negative damping coefficients lead to multiple equilibria or energy growth and were not analyzed. Fourth, the equivalent-damping relation (16) and the explanation of the peak delay are approximate interpretations, not derived bounds. Fifth, the analysis does not give an explicit global decay rate; obtaining a strict Lyapunov function with a quantitative convergence estimate would require additional work. Finally, the γ sweep used six values and one initial condition, so the observed monotone trends should not be extrapolated beyond that range.

IX. CONCLUSION

A nonlinear oscillator with linear and cubic velocity damping and hardening cubic stiffness was analyzed mathematically and numerically. Under $m > 0$, $k > 0$, $\alpha \geq 0$, $c \geq 0$, $\gamma \geq 0$ and $c + \gamma > 0$, the origin is the unique equilibrium. Its linearization has eigenvalues $\left(-c \pm \sqrt{c^2 - 4mk}\right)/(2m)$, which equal $-0.075 \pm 0.99718\,i$ for the nominal parameters and do not depend on γ. The mechanical energy satisfies $\dot{E} = -cv^2 - \gamma v^4 \leq 0$, and LaSalle's invariance principle shows that the origin is globally asymptotically stable, including the non-hyperbolic case $c = 0, \gamma > 0$.

High-accuracy simulations with the DOP853 integrator were consistent with these results. Energy decreased monotonically in all runs, and the computed energy rate and integrated energy balance agreed with the analytical expressions to within the expected numerical error. For the studied parameters, the cubic damping term lowered the energy remaining at $t = 30$ by about 9%, 32% and 58% for initial displacements 0.5, 1.0 and 1.5. This growing effect with amplitude agrees qualitatively with the equivalent damping $c + 3/4\,\gamma A^2\omega^2$. Increasing γ reduced peak amplitudes monotonically and slightly delayed successive peaks. Near equilibrium, decay was governed by the linear damping, as the linearization predicts.

Natural extensions are the forced response, parameter identification from measured data, the softening case $\alpha < 0$, and a quantitative convergence-rate estimate for the case $c = 0$.

REFERENCES

[1] S. H. Strogatz, *Nonlinear Dynamics and Chaos: With Applications to Physics, Biology, Chemistry, and Engineering*, 2nd ed. Boulder, CO, USA: Westview Press, 2015.

[2] H. K. Khalil, *Nonlinear Systems*, 3rd ed. Upper Saddle River, NJ, USA: Prentice Hall, 2002.

[3] A. H. Nayfeh and D. T. Mook, *Nonlinear Oscillations*. New York, NY, USA: Wiley, 1979.

[4] I. Kovacic and M. J. Brennan, Eds., *The Duffing Equation: Nonlinear Oscillators and their Behaviour*. Chichester, U.K.: Wiley, 2011, doi: 10.1002/9780470977859.

[5] A. M. Lyapunov, "The general problem of the stability of motion," *Int. J. Control*, vol. 55, no. 3, pp. 531–534, 1992 (English translation of the 1892 thesis), doi: 10.1080/00207179208934253.

[6] J. P. LaSalle, "Some extensions of Liapunov's second method," *IRE Trans. Circuit Theory*, vol. 7, no. 4, pp. 520–527, Dec. 1960, doi: 10.1109/TCT.1960.1086720.

[7] A. Eichler, J. Moser, J. Chaste, M. Zdrojek, I. Wilson-Rae, and A. Bachtold, "Nonlinear damping in mechanical resonators made from carbon nanotubes and graphene," *Nature Nanotechnol.*, vol. 6, no. 6, pp. 339–342, 2011, doi: 10.1038/nnano.2011.71.

[8] L. Catalini, M. Rossi, E. C. Langman, and A. Schliesser, "Modeling and observation of nonlinear damping in dissipation-diluted nanomechanical resonators," *Phys. Rev. Lett.*, vol. 126, Art. no. 174101, 2021, doi: 10.1103/PhysRevLett.126.174101.

[9] Z. Q. Lang, X. J. Jing, S. A. Billings, G. R. Tomlinson, and Z. K. Peng, "Theoretical study of the effects of nonlinear viscous damping on vibration isolation of sdof systems," *J. Sound Vib.*, vol. 323, no. 1–2, pp. 352–365, 2009, doi: 10.1016/j.jsv.2009.01.001.

[10] Z. Xiao, X. Jing, and L. Cheng, "The transmissibility of vibration isolators with cubic nonlinear damping under both force and base excitations," *J. Sound Vib.*, vol. 332, no. 5, pp. 1335–1354, 2013, doi: 10.1016/j.jsv.2012.11.001.

[11] B. Tang and M. J. Brennan, "A comparison of the effects of nonlinear damping on the free vibration of a single-degree-of-freedom system," *J. Vib. Acoust.*, vol. 134, no. 2, Art. no. 024501, 2012, doi: 10.1115/1.4005010.

[12] S. J. Elliott, M. Ghandchi Tehrani, and R. S. Langley, "Nonlinear damping and quasi-linear modelling," *Phil. Trans. R. Soc. A*, vol. 373, no. 2051, Art. no. 20140402, 2015, doi: 10.1098/rsta.2014.0402.

[13] Y.-P. Zhu and Z. Q. Lang, "Beneficial effects of antisymmetric nonlinear damping with application to energy harvesting and vibration isolation under general inputs," *Nonlinear Dyn.*, vol. 108, no. 4, pp. 2917–2933, 2022, doi: 10.1007/s11071-022-07444-0.

[14] Y. O. El-Dib, "The damping Helmholtz–Rayleigh–Duffing oscillator with the non-perturbative approach," *Math. Comput. Simul.*, vol. 194, pp. 552–562, 2022, doi: 10.1016/j.matcom.2021.12.014.

[15] A. H. Salas, "An elementary solution to a Duffing equation," *Sci. World J.*, vol. 2022, Art. no. 2357258, 2022, doi: 10.1155/2022/2357258.

[16] G. M. Moatimid, T. S. Amer, and W. S. Amer, "Dynamical analysis of a damped harmonic forced Duffing oscillator with time delay," *Sci. Rep.*, vol. 13, Art. no. 6507, 2023, doi: 10.1038/s41598-023-33461-z.

[17] K. Alluhydan, G. M. Moatimid, T. S. Amer, and A. A. Galal, "Inspection of a time-delayed excited damping Duffing oscillator," *Axioms*, vol. 13, no. 6, Art. no. 416, 2024, doi: 10.3390/axioms13060416.

[18] M. K. Abohamer, T. S. Amer, A. Arab, and A. A. Galal, "Analyzing the chaotic and stability behavior of a Duffing oscillator excited by a sinusoidal external force," *J. Low Freq. Noise Vib. Active Control*, vol. 44, no. 2, 2025, doi: 10.1177/14613484241298998.

[19] P. Kakou, S. K. Gupta, and O. Barry, "A nonlinear analysis of a Duffing oscillator with a nonlinear electromagnetic vibration absorber–inerter for concurrent vibration mitigation and energy harvesting," *Nonlinear Dyn.*, vol. 112, no. 8, pp. 5847–5862, 2024, doi: 10.1007/s11071-023-09163-6.

[20] J. R. Dormand and P. J. Prince, "A family of embedded Runge–Kutta formulae," *J. Comput. Appl. Math.*, vol. 6, no. 1, pp. 19–26, 1980, doi: 10.1016/0771-050X(80)90013-3.

[21] E. Hairer, S. P. Nørsett, and G. Wanner, *Solving Ordinary Differential Equations I: Nonstiff Problems*, 2nd rev. ed., ser. Springer Series in Computational Mathematics, vol. 8. Berlin, Germany: Springer, 1993, doi: 10.1007/978-3-540-78862-1.

[22] P. Virtanen *et al.*, "SciPy 1.0: Fundamental algorithms for scientific computing in Python," *Nature Methods*, vol. 17, no. 3, pp. 261–272, 2020, doi: 10.1038/s41592-019-0686-2.

[23] C. R. Harris *et al.*, "Array programming with NumPy," *Nature*, vol. 585, no. 7825, pp. 357–362, 2020, doi: 10.1038/s41586-020-2649-2.

[24] J. D. Hunter, "Matplotlib: A 2D graphics environment," *Comput. Sci. Eng.*, vol. 9, no. 3, pp. 90–95, 2007, doi: 10.1109/MCSE.2007.55.